Photoelectron spectroscopy of the thiazate (NSO^-) and thionitrite (SNO^-) isomer anions

Julia H. Lehman and W. Carl Lineberger

Citation: The Journal of Chemical Physics **147**, 013943 (2017); doi: 10.1063/1.4984129
View online: http://dx.doi.org/10.1063/1.4984129
View Table of Contents: http://aip.scitation.org/toc/jcp/147/1
Published by the American Institute of Physics

Photoelectron spectroscopy of the thiazate (NSO^-) and thionitrite (SNO^-) isomer anions

Julia H. Lehman[a),b)] and W. Carl Lineberger[b)]
JILA and Department of Chemistry and Biochemistry, University of Colorado, Boulder, Colorado 80309, USA

(Received 15 March 2017; accepted 12 May 2017; published online 6 June 2017)

Anion photoelectron spectra of the thiazate (NSO^-) and thionitrite (SNO^-) isomers are reported. The NSO^- photoelectron spectrum showed several well-resolved vibronic transitions from the anion to the NSO radical neutral. The electron affinity of NSO was determined to be 3.113(1) eV. The fundamental vibrational frequencies of NSO were measured and unambiguously assigned to be 1202(6) cm^{-1} (ν_1, asymmetric stretch), 1010(10) cm^{-1} (ν_2, symmetric stretch), and 300(7) cm^{-1} (ν_3, bend). From the presence of vibrational hot band transitions, the fundamental vibrational frequencies of the NSO^- anion were also measured: 1280(30) cm^{-1} (ν_1, asymmetric stretch), 990(20) cm^{-1} (ν_2, symmetric stretch), and 480(10) cm^{-1} (ν_3, bend). Combined with the previously measured $\Delta_{acid}H^{o}_{298\ K}$(HNSO), D_0(H–NSO) was found to be 102(5) kcal/mol. Unlike the results from NSO^-, the SNO^- photoelectron spectrum was broad with little structure, indicative of a large geometry change between the anion and neutral radical. In addition to the spectrally congested spectrum, there was evidence of a competition between photodetachment from SNO^- and SNO^- photodissociation to form S^- + NO. Quantum chemical calculations were used to aid in the interpretation of the experimental data and agree well with the observed photoelectron spectra, particularly for the NSO^- isomer. *Published by AIP Publishing.* [http://dx.doi.org/10.1063/1.4984129]

I. INTRODUCTION

Chalcogen-nitrogen chemistry has a rich scientific history, particularly involving the chemistry of S–N compounds and their importance as linkage isomers in transition metal complexes.[1] Recently, s-nitrosothiols (RSNO, where R is an alkyl group) and perthionitrite ($SSNO^-$) have been implicated in biological signaling, specifically in the storage and transport of nitric oxide in biological systems.[2–6] The isomeric acids HSNO and HNSO have been the focus of several recent experimental and theoretical studies,[7–12] primarily due to their potential involvement in these biological processes. However, surprisingly little is experimentally known about their conjugate bases, thionitrite (SNO^-) and its energetically more stable isomer thionylimide or thiazate anion (NSO^-), or even the properties of their corresponding neutral radicals (SNO and NSO).

For a set of "simple" triatomic molecules, SNO and NSO (along with their anions) have proven to be difficult to isolate and study experimentally. Several matrix isolation experiments have measured the infrared spectra of SNO and its more energetically stable isomer NSO, although not without some controversy over vibrational band assignments.[13–18] A common theme of these studies is that SNO or NSO was observed as a decomposition product of other S, N, and O containing molecules. Early assignments of the stretching vibrational frequencies of SNO and NSO came from Tchir and Sprately,[13,14] where isomers of HSNO were formed in an argon matrix and, following UV irradiation, several new vibrational absorption peaks were observed. Some of these peaks were then attributed to either SNO or NSO, resulting in an assignment of the NO stretch and SNO bend vibrational frequencies of SNO[13] and the SO stretching frequency for NSO.[14] It was later suggested that the initial assignments of SNO vibrational frequencies were better matched to the SN and NO stretches, rather than the NO stretch and SNO bend.[18] In addition, the SO stretching frequency for NSO had a larger than expected isotopic shift,[14,15] which called into question its identification. Most recently, Wu *et al.* produced NSO from the 600 K decomposition of $CF_3S(O)N$, which was then deposited onto argon and neon matrices.[15] Two vibrational frequencies were identified, 1199.3 and 995.4 cm^{-1} (Ne matrix), as belonging to the two stretching modes of NSO, but were assigned as the symmetric and asymmetric stretches, respectively, inconsistent with previous work. In addition, the two stretching modes of SNO (1603.6 and 792.3 cm^{-1}) were observed following irradiation of the neon matrix at 193 nm, agreeing well with the previous argon matrix studies. However, the NSO and SNO radicals have yet to be observed in the gas phase, and therefore there are still questions about the vibrational mode assignments.

There have also been theoretical studies examining the electronic structure and vibrational frequencies of the NSO and SNO radical neutral molecules.[16,17,19,20] Some of these studies were done in support of the matrix-isolation experiments.[16,17] Recent work from Yazidi *et al.*[20] and Trabelsi *et al.*[19] also explored the electronic structure of the neutral radicals at a much higher level of theory than previously done [MRCI in Ref. 20 and CCSD(T) with an extrapolation to the complete basis set limit in Ref. 19]. There is significantly more

[a)] Present address: School of Chemistry, University of Leeds, Leeds LS2 9JT, United Kingdom.
[b)] Authors to whom correspondence should be addressed: J.Lehman@Leeds.ac.uk and Carl.Lineberger@Colorado.edu

theoretical knowledge about the NSO^- and SNO^- anions than their corresponding neutral radicals,[19,21–24] including in-depth studies into their role in coordination chemistry and their use as linkage isomers (see Ref. 21 or Ref. 22 and references therein for additional information).

The experimental measurement of fundamental properties of NSO and SNO, including their electron affinities and vibrational frequencies, is essential for the validation of the theoretical methods used to treat these radicals, particularly because of their role as small building blocks for larger, substituted thionylimide or sulfinylnitrene molecules. This experiment uses photoelectron spectroscopy of NSO^- to experimentally measure the electron affinity (EA) and vibrational frequencies of the NSO radical neutral. Vibrational frequencies of the NSO^- anion are also measured. The NSO^- and SNO^- anions are able to be independently formed without significant isomeric contamination using rational ion synthesis in our dual-valve pulsed plasma entrainment ion source. The measured NSO^- photoelectron spectrum proves to be straightforward to analyze and yields an abundance of information. However, the SNO^- photoelectron spectrum exhibits significant spectral congestion, making interpretation challenging and again showcasing how understanding these "simple" triatomic molecules can be a non-trivial problem for experiment and theory alike.

II. EXPERIMENTAL METHODS

The experimental apparatus has been described in detail previously,[25] so only a brief description follows. Anions are generated in a dual pulsed valve plasma entrainment ion source,[26] discussed further below. Briefly, two pulsed General Valves are used to generate and collisionally stabilize the products from rational ion synthesis. The two valves, oriented perpendicular to each other, are referred to as the side and main gas expansions. The side gas expansion is operated in such a way to produce a low flow of gas, resulting in approximately an order of magnitude lower chamber pressure rise during normal operating conditions compared to the main gas expansion. This valve features a pulsed parallel plate discharge, which generates plasma. The plasma is entrained into the main supersonic expansion, which primarily consists of argon, where the ions are collisionally cooled and stabilized. The anions are extracted downstream from the ion source into a Wiley-McLaren time-of-flight (TOF) mass spectrometer. Here, the anions are separated by their mass-to-charge (m/z) ratio, focused, and steered into the laser-ion interaction region. The third harmonic of an Nd:YAG laser (355 nm, 3.4945 eV) spatially and temporally overlaps the anion m/z of interest, detaching electrons. The three dimensional velocity distribution of photodetached electrons is velocity-mapped onto a microchannel plate detector coupled to a phosphor screen,[27] resulting in a two dimensional image of the three dimensional electron velocity distribution. The image is reconstructed using the BASEX algorithm,[28] resulting in a one-dimensional photoelectron velocity distribution, which is then transformed into an electron kinetic energy (eKE) distribution via a Jacobian transformation. The eKE scale is calibrated by the known photoelectron spectrum of the atomic anion S^-.[29,30] Due to the nature of the velocity map imaging (VMI) spectrometer, the instrument resolution is a function of the eKE and is approximately constant at very low eKE (<100 meV). Based on the S^- photoelectron spectrum, the instrument resolution is approximately 2.8% ΔE/eKE, where ΔE is the full-width-at-half-maximum (*fwhm*) of the peaks in the S^- photoelectron spectrum. At very low eKE (<100 meV), the instrument achieves approximately 3 meV resolution. In this work, the photoelectron spectra are reported as electron binding energy (eBE), where eBE = hν − eKE.

While most of the reported spectra were taken using 355 nm photons, additional experiments were done using other photon energies. Specifically, the second harmonic of the Nd:YAG laser was used directly (532 nm), and in another study, the output from a 355 nm pumped visible optical parametric oscillator (OPO) was used (477.6 nm, or 2.596 eV). The highest photon energy used was 3.669 eV, which was generated from doubling the output of a 532 nm pumped dye laser (LDS 698).

The anions of interest, NSO^- and SNO^-, are generated through rational ion synthesis in our dual valve ion source.[26] An isomer-specific method for generating NSO^- and SNO^- is necessary in order for this experiment to be successful. The reaction of NH_2^- with SO_2 is used for the generation of NSO^-.[31] Here, NH_2^- is formed from a pulsed discharge of 10% NH_3 (balance Ar) in the side gas expansion. This reacts with a trace amount (<0.5%) of SO_2 in the main supersonic expansion of argon, forming NSO^-. The reaction product is collisionally cooled and stabilized. From the room temperature selected ion flow tube reaction from Bierbaum *et al.*,[31] this reaction was shown to produce m/z = 62 with a branching fraction of 26%. The anion at m/z = 62 was hypothesized to be NSO^- based on a probable mechanism and measured gas-phase acidity. In the current experiment, this reaction product is confirmed and no evidence is seen for other isomers of the same mass being formed from this reaction, as shown in Sec. III A.

The association reaction of S^- with NO was used to generate the SNO^- isomer. In the side expansion, S^- is generated from the pulsed discharge of the vapor from room temperature CS_2 entrained in Ar (approximately 25% CS_2, balance Ar). A trace amount (<0.5%) of NO was added to the main expansion of Ar. The nitric oxide mixture is further purified using a copper coil that is submerged in a dry ice/methanol bath and is filled with Ascarite, similar to the procedure from Van Doren *et al.*[32] The reaction of S^- with NO results in either SNO^- or NOS^- being formed. From the results discussed below, it is evident that the primary product is SNO^-. No evidence is seen for NSO^- or other isomers at m/z = 62 generated from this method in the current experiment.

Calculations are performed to aid in the analysis of the experimental photoelectron spectra. The Gaussian suite of programs[33] was used to calculate and optimize energies, geometries, and harmonic frequencies of NSO^-, NSO, SNO^-, SNO, NOS^-, and NOS at the B3LYP/aug-cc-pVTQZ level of theory (ROB3LYP for neutral radicals). The calculated geometries, normal mode vectors, and the harmonic vibrational frequencies are used to calculate the Franck-Condon factors (FCFs)

for the simulated photoelectron spectra using the PESCAL program.[34,35] The FCFs are convolved with Gaussian functions whose width is the instrument resolution and whose integrated intensity is equal to the calculated FCF. Again, the instrument resolution is from the S^- photoelectron spectrum calibration, yielding *fwhm* ~ 2.8% ΔE/eKE. The sum of these Gaussian functions is the simulated (convolved) photoelectron spectrum. For the calculated FCFs, the anion is assumed to have a vibrational temperature of 200 K, resulting in transitions from excited vibrational states of the anion to vibrational states of the neutral (hot bands and/or sequence bands).

Throughout this paper, only the ground electronic states of these anions and neutral radicals are discussed, so the ground electronic state designations are not referred to in order to help simplify the written explanations. The vibrational frequencies reported here for NSO^- and NSO follow the convention of ν_1, ν_2, and ν_3 labeled as what can best be described as the asymmetric stretch, symmetric stretch, and bending frequencies, respectively. However, ν_1 and ν_2 of the neutral NSO can also be referred to as the SO stretch and NS stretch, respectively, given the displacement vectors calculated here (B3LYP/aug-cc-pVQZ) and reported in the supplementary material. For the SNO isomer, the vibrational modes are better described as ν_1 as the NO stretch, ν_2 as the SN stretch, and ν_3 as the SNO bend. The vibronic transition assignments are labeled as the number of quanta in each vibration, $(\nu_1, \nu_2, \nu_3)_{neutral} \leftarrow (\nu_1, \nu_2, \nu_3)_{anion}$.

The error bars throughout this work are calculated based on the statistical error in determining the photoelectron energy corresponding to a peak center, possible contributions of multiple transitions to an individual peak, the error in the absolute energy scale calibration (when a contributor), and multiple independent measurements of the photoelectron spectra. The error in the absolute energy scale calibration is not necessary to include for energy differences between peaks, such as the vibrational frequencies reported here. Any additional error derived from the difference between the observed peak center and the underlying vibronic transition is included in the error analysis and is explicitly stated in Secs. III and IV; causes of additional error include an asymmetric, unresolved rotational contour or if there are multiple vibronic transitions possible for what appears to be a single observed peak.

III. RESULTS

A. NSO^- photoelectron spectrum

The doubly occupied HOMO of NSO^- has both bonding and antibonding character: it is bonding in the N–S bond and antibonding in the S–O bond.[11,19] When an electron is removed from this orbital, generating the radical neutral NSO in its ground electronic state, it is expected that the N–S bond should lengthen (less bonding character) and the S–O bond should shorten (less antibonding character) due to the change in the bond order. This is seen in the calculated geometries of NSO^- and NSO summarized in Table I. The anti-correlated change in bond lengths will likely be reflected in Franck-Condon activity in the asymmetric stretching vibration. However, based on the relatively small difference between the equilibrium geometries of the anion and neutral (approximately 3% change in the bond lengths, <1% change in the angle), the photoelectron spectrum will likely show a vertical transition. In other words, it is expected that the most intense transition will be from the ground vibrational state of the anion to the ground vibrational state of the neutral (otherwise known as the peak corresponding to the electron affinity, EA) with very little Franck-Condon activity otherwise.

TABLE I. Calculated geometries and harmonic frequencies for NSO^-, NSO, SNO^-, and SNO (B3LYP/aug-cc-pVQZ, ROB3LYP for the neutral radicals). The differences between the anion and neutral geometries are shown in the last column, with the percent change from the anion shown in parentheses. The calculated electron affinities (EAs) for NSO and SNO are also included.

	NSO^-	NSO	Δ(anion-neutral)
r(N–SO) (Å)	1.479	1.511	−0.037 (−2.5%)
r(NS–O) (Å)	1.510	1.464	0.047 (3.1%)
∠ (NSO) (deg)	123.2	122.7	0.4 (0.3%)
ω_1 (cm^{-1})	1283.8	1199.1	...
ω_2 (cm^{-1})	993.2	1017.2	...
ω_3 (cm^{-1})	486.8	313.9	...
EA (eV)	...	3.025	...
	SNO^-	SNO	Δ(anion-neutral)
r(S–NO) (Å)	1.717	1.585	0.132 (7.7%)
r(SN–O) (Å)	1.229	1.185	0.044 (3.6%)
∠(SNO) (deg)	118.7	140.1	−21.4 (−18.1%)
ω_1 (cm^{-1})	1405.3	1645.8	...
ω_2 (cm^{-1})	720.4	813.5	...
ω_3 (cm^{-1})	489.4	510.9	...
EA (eV)	...	2.113	...

The experimental photoelectron spectrum of NSO^- using 355 nm photons is shown as the black line in Fig. 1, with the raw (unreconstructed) velocity-mapped photoelectron image shown in the inset. As expected, there are very few peaks with significant intensity. The dominant peak in the spectrum is the transition from the ground vibrational state of the anion to the ground vibrational state of the neutral, or the electron affinity (EA) of NSO. This peak is located at 3.113(1) eV. The *fwhm* of this peak (0.014 eV) is slightly broader than the instrument limited resolution, which is 0.011 eV at this eKE. This is most likely due to an underlying rotational contour, causing a broadening of this peak. The center of the observed peak does not necessarily have to correspond to the transition energy due to an unresolved rotational contour. An estimate of the offset between the peak center and the EA transition energy is based on the calculated rotational constants of the anion and neutral and an assumed rotational temperature of 150(50) K.[36] The resulting offset is very small (approximately 0.2 meV). This small approximate shift has been further confirmed using a rotational contour simulated in PGOPHER using the calculated rotational constants.[37] Taking this offset and its associated error into account results in the EA(NSO) = 3.113(1). The calculated (B3LYP/aug-cc-pVQZ) EA of 3.025 eV agrees well with the experimental value.

The remaining peaks in the spectrum are assigned with the aid of the calculated photoelectron simulation, which overall

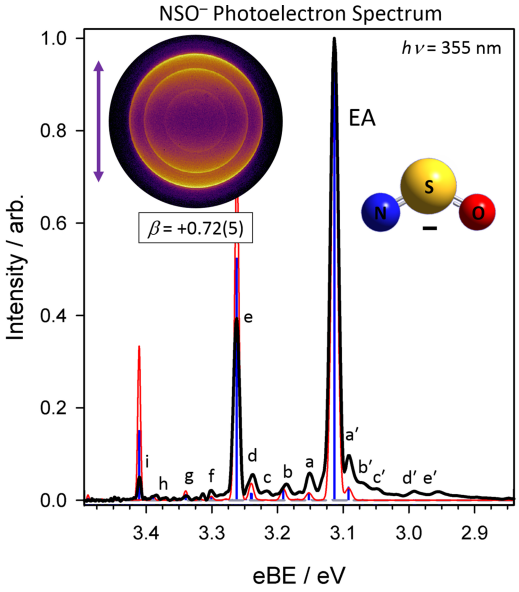

FIG. 1. Experimental photoelectron spectrum of NSO^- using 355 nm (3.49 eV) photon energy, shown in black. The inset is the raw (not reconstructed) velocity-mapped photoelectron image, with the direction of the laser polarization shown as the purple double-headed arrow. The anisotropy parameter (β) is reported for the peak corresponding to the EA. The peak labels (letters) are referred to in the main text and in Table II. The calculated Franck-Condon factors for the photodetachment from NSO^- are shown as blue sticks. The convolution of the Franck-Condon factors with the experimental resolution, as discussed in the text, is shown as the red line.

TABLE II. Summary of peaks identified in the NSO^- photoelectron spectrum, using peak labels found in Fig. 1. Absolute peak positions (eBE, reported in eV), vibrational transition frequency based on the peak position relative to the EA (cm^{-1}), and the vibrational transition assignments are listed. The vibronic transition assignments are listed as the number of quanta in each vibration, $(\nu_1, \nu_2, \nu_3)_{neutral} \leftarrow (\nu_1, \nu_2, \nu_3)_{anion}$, where ν_1, ν_2, ν_3 are the asymmetric stretch, symmetric stretch, and bending vibrations, respectively. The transition frequencies are measured relative to the EA. The asterisks for peaks c and h indicate the inability to clearly assign these peaks to a single transition.

Peak label	Peak position (eV)	Vibrational transition frequency (cm^{-1})	Vibronic transition assignment
e′	2.955(2)	1280(30)	(0, 0, 0) ← (1, 0, 0)
d′	2.990(2)	990(25)	(0, 0, 0) ← (0, 1, 0)
c′	3.049(2)	510(25)	(0, 0, 0) ← (0, 0, 1)
b′	3.071(2)	320(20)	(0, 0, 2) ← (0, 0, 2)
a′	3.091(1)	180(10)	(0, 0, 1) ← (0, 0, 1)
EA	3.113(1)	0	(0, 0, 0) ← (0, 0, 0)
a	3.151(1)	300(7)	(0, 0, 1) ← (0, 0, 0)
b	3.187(1)	593(7)	(0, 0, 2) ← (0, 0, 0)
c	3.217(1)	840(10)	*
d	3.238(1)	1010(10)	(0, 1, 0) ← (0, 0, 0)
e	3.262(1)	1202(6)	(1, 0, 0) ← (0, 0, 0)
f	3.300(1)	1508(8)	(1, 0, 1) ← (0, 0, 0)
g	3.339(1)	1822(7)	(1, 0, 2) ← (0, 0, 0)
h	3.385(1)	2190(10)	*
i	3.410(1)	2394(6)	(2, 0, 0) ← (0, 0, 0)

agrees very well with the experimental spectrum. Note that the simulation was shifted by +88 meV to match the experimental EA(NSO). A higher photon energy (3.669 eV) was also used, but no additional peaks were observed to higher binding energy. A comparison of the photoelectron spectra resulting from the two different photon energies is shown in the supplementary material. The results of the peak assignments are listed in Table II. Peaks corresponding to transitions from the ground vibrational state of the anion to the asymmetric, symmetric, and bending vibrations of the neutral will be discussed first in the paragraphs below. This will be followed by identifying hot band and sequence band progressions (transitions from excited vibrational states of the anion to different vibrational states of the neutral).

Peak e is the second largest peak in the photoelectron spectrum after the EA. It is spaced by approximately 1200 cm^{-1} relative to the EA. Peak i is spaced by approximately 1190 cm^{-1} from peak e (approximately 2390 cm^{-1} from the EA). These two peaks are assigned as transitions from the ground vibrational state of the anion to one and two quanta of asymmetric stretch in the neutral NSO, respectively, yielding a measurement of the fundamental ν_1 = 1202(6) cm^{-1} and the overtone $2\nu_1$ = 2394(6) cm^{-1} vibrational frequencies. The measured frequency agrees very well with the harmonic frequency calculation (ROB3LYP/aug-cc-pVQZ) of 1199 cm^{-1}. As expected from the change in the bonding character and the associated change in the geometry between the anion and neutral, this progression in the asymmetric stretch has the largest Franck-Condon activity.

Peak d is spaced from the EA peak by 1010 cm^{-1}. The major contribution to the peak intensity is predicted to be the transition from the ground vibrational state of the anion to one quantum in the NSO symmetric stretch. However, the peak is also predicted to have small contributions from other vibronic transitions which are distributed nonsymmetrically about the primary transition. This gives rise to the non-Gaussian peak shape. A larger error bar is therefore used for the NSO symmetric stretch transition frequency to help account for the added uncertainty. The NSO symmetric stretch (ν_2) is identified as 1010(10) cm^{-1}. This agrees very well with the harmonic frequency calculation (ROB3LYP/aug-cc-pVQZ) of 1017 cm^{-1}.

The final NSO frequency which is able to be measured is for the bending vibration. There are a set of small peaks attributed to the transition from the ground vibrational state of the anion to one and two quanta in the NSO bend: peaks a and b, respectively. From the position of these peaks relative to the EA, the fundamental frequency of the NSO bend (ν_3) is identified as 300(7) cm^{-1} and the overtone ($2\nu_3$) as 593(7) cm^{-1}. Again, this agrees very well with the calculated (ROB3LYP/aug-cc-pVQZ) harmonic frequency of 314 cm^{-1}. There are also a few combination bands that are observed, involving transitions from the ground vibrational state of the anion to one quantum in the NSO asymmetric stretch, plus one or two quanta in the NSO bend (peaks f and g, respectively). These neutral vibrational frequencies are measured as $\nu_1 + \nu_3$ = 1508(8) cm^{-1} and $\nu_1 + 2\nu_3$ = 1822(7) cm^{-1}.

Beyond being able to determine neutral NSO vibrational frequencies, some frequencies of the NSO^- anion were also able to be measured. There are several small peaks to lower eBE than the peak assigned as the EA. These are attributed to vibrational hot bands, i.e., transitions arising from excited vibrational states of the anion to the ground vibrational state

of the neutral. Peak e′ is assigned to the transition from one quantum of the anion asymmetric stretch to the ground state of the neutral. It is located approximately 1280 cm^{-1} from the EA. Peak d′ is assigned to the transition from one quanta of the anion symmetric stretch to the ground state of the neutral. It is located approximately 990 cm^{-1} from the EA. Both of these peaks have fairly low intensity and are significantly broader than the experimental resolution. There are numerous transitions predicted to form these peaks, which is likely the cause for the breadth of the peaks. However, because of this added uncertainty, a conservative error is used for both of these anion frequencies: 1280(30) cm^{-1} and 990(25) cm^{-1} for the anion ν_1 and ν_2, respectively. These agree very well with the calculated (B3LYP/aug-cc-pVQZ) harmonic frequencies of 1284 cm^{-1} and 993 cm^{-1}.

There are also several sequence bands present for the bending vibration, i.e., transitions from one or two quanta of bend in the anion to one or two quanta of bend in the neutral. The largest peak to lower eBE than the EA (peak a′) is assigned as the (0,0,1) ← (0,0,1) sequence band. From this peak position, combined with the measured frequency of the neutral ν_3 fundamental vibration, the anion ν_3 is measured to be 480(10) cm^{-1}. The calculated (B3LYP/aug-cc-pVQZ) harmonic frequency of 487 cm^{-1} agrees with this very well. An additional sequence band, assigned to the (0,0,2) ← (0,0,2) transition, is labeled as peak b′. From this peak position combined with the measurement of the neutral $2\nu_3$, the anion $2\nu_3$ is measured as 910(20) cm^{-1}. A direct measurement of the anion ν_3 has more uncertainty associated with it because of peak shapes and intensities. Peak c′ is assigned as the transition from one quantum in the anion bend to the vibrational ground state of the neutral. However, given the peak shape and nearby peaks interfering with an accurate measure of its position, a larger error bar is placed on the anion ν_3 measured this way, yielding 510(25) cm^{-1}. This is similar to the value derived from the observed sequence band, but with a larger error.

It is apparent from the image that there is an angular anisotropy of the photoelectrons with respect to the direction of the laser polarization (double headed arrow). Within the BASEX algorithm, the photoelectron intensity as a function of the polar angle (θ) with respect to the laser polarization is fit to the form: $I(\theta) \propto 1 + \beta P_2(\cos\theta)$. The anisotropy parameter (β) ranges from −1 for a perpendicular transition to +2 for a parallel transition. Generally, for photoelectron spectroscopy of molecular anions,[38] a positive β is associated with detachment from an orbital with more σ character, while a negative β is associated with detachment from a more π like orbital. In the NSO^- image, the most intense peak (the EA) has $\beta \approx +0.7$, indicating that electron detachment is from an orbital with more σ character. This is consistent with the anion HOMO being associated with σ-like bonds.

B. SNO^- photoelectron spectrum

By employing a different ion synthesis method in our ion source, we are able to switch from generating NSO^- to another S, N, O containing anion at m/z = 62. This was achieved by reacting S^- with NO, as explained in Sec. II. There are two possible isomers that could be formed from the reaction of S^- with NO: SNO^- or NOS^-. The NSO^- anion is not observed, which is anticipated, based on the significant structural rearrangement that would need to occur, including breaking the NO bond. For either possible isomer, the central atom is no longer the least electronegative atom, which will likely destabilize these isomers compared to NSO^-. Indeed, the SNO^- anion is calculated to be energetically less stable than NSO^- by approximately 1 eV.[19,23] In addition, the NOS^- anion is calculated to be 2.14 eV higher in energy than SNO^- (B3LYP/aug-cc-pVQZ). The transition state for the rearrangement between NOS^- and SNO^- is almost 1 eV higher in energy than NOS^-. The energetic difference between NOS^- and SNO^- does not necessarily preclude NOS^- from existing in our mass spectrum, but it is certainly less likely. In addition, based on the calculations done here (B3LYP/aug-cc-pVQZ), the reaction of S^- with NO is slightly endothermic for producing NOS^- (by approximately 0.2 eV) and exothermic for producing SNO^- (by about 1.9 eV). This again points to SNO^- being the most likely isomer to be formed in this ion source.

Assuming that SNO^- is the only ion produced at m/z = 62, it is instructive to postulate what the photoelectron spectrum might look like. According to the notation from Ehrhardt and Ahlrichs,[23] the electronic structure of SNO^- can best be described as $S^- - N = O$, as opposed to NSO^- which can be described as $N^- = S^+ - O^-$. From the current calculations, there is a significant change in geometry between the anion and neutral SNO, summarized in Table I. While the SNO angle is the most significant change (~20% change), the two bond lengths also show small changes. Therefore, an extended vibrational progression is expected in the photoelectron spectrum. The calculated vibrational frequencies are also reported in Table I.

The photoelectron spectrum of SNO^- is shown in Fig. 2, using 355 nm photons. The experimental spectrum shows two fairly sharp peaks (at approximately 2.1 and 3.25 eV). The two sets of peaks are readily assigned to the photodetachment from S^- (^2P) to form S (^3P) and S (^1D). The presence of these peaks will be discussed below. There is also a broad, somewhat structured "feature" spanning more than 1 eV, centered near 2.7 eV. This broad "feature" also causes a vertical offset in the amplitude of the photodetachment from S^- (^2P) to form S (^1D). The photoelectron angular distribution for this portion of the spectrum showed a positive anisotropy ($\beta \approx +0.4$ over the *fwhm* of the spectrum), once again indicating the photodetachment from a more σ-like orbital. A broad spectrum like what is seen here is indicative of a large geometry change between the anion and neutral molecules, resulting in a spectrally congested spectrum. The SNO^- photoelectron spectrum simulation is overlaid on the experimental spectrum. Here, the calculated EA (2.113 eV) is shifted by +50 meV in order to better match the peak of the experimental spectrum at 2.7 eV, otherwise known as the vertical detachment energy (VDE). Overall, the simulation agrees fairly well with the experiment, particularly given the degree of spectral congestion.

In order to trying to identify individual transitions and hopefully identifying the EA, a lower photon energy was used (477.6 nm, or 2.596 eV). Since the experimental

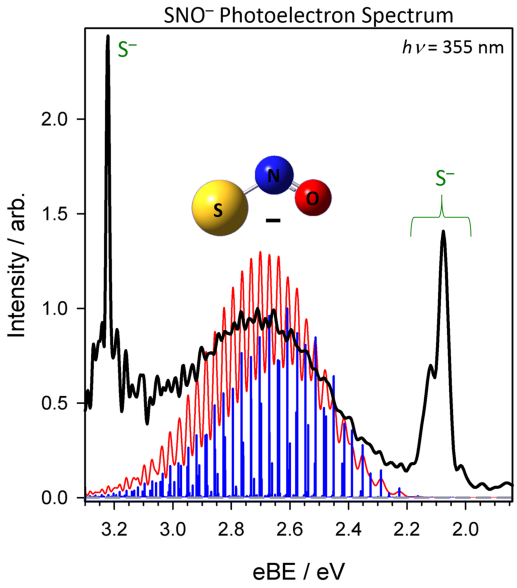

FIG. 2. Experimental photoelectron spectrum of SNO^- using 355 nm (3.49 eV) photon energy, shown in black. The broad, semi-structured peak centered at 2.7 eV is attributed to SNO^-, while the two peaks at approximately 2.1 eV and 3.2 eV are from the S^- photodetachment, arising from a two-photon process: SNO^- photodissociation to S^- + NO, followed by the S^- photodetachment, as discussed in the text. The calculated Franck-Condon factors for the SNO^- photodetachment are shown as blue sticks. The convolution of the Franck-Condon factors with the experimental resolution, as discussed in the text, is shown as a red line.

resolution changes as a function of eKE, a lower photon energy should help better resolve the low eBE portion of the spectrum despite the spectral congestion. The resulting spectrum is shown in Fig. 3. The four peaks near 2.1 eV are again assigned to the photodetachment from S^- (^{2}P)

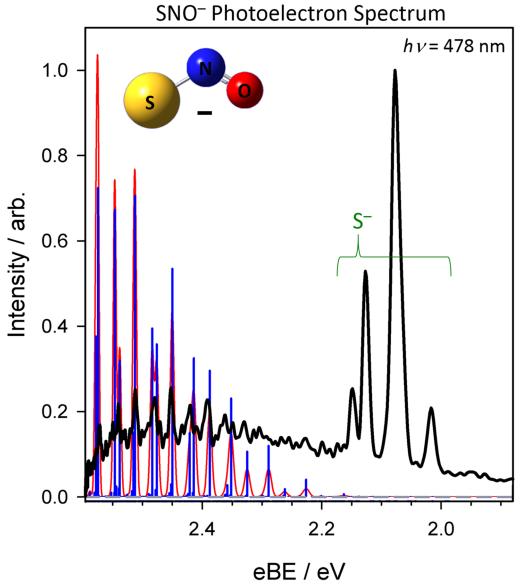

FIG. 3. Experimental photoelectron spectrum of SNO^- using 478 nm (2.596 eV) photon energy, shown in black. With a lower photon energy, the broad peak centered at 2.7 eV in Fig. 2 is now better resolved, showing evidence of some structure. The peaks between 2 and 2.15 eV are due to the photodetachment from S^-. The calculated Franck-Condon factors for the photodetachment from SNO^- are shown as blue sticks. The convolution of the Franck-Condon factors with the experimental resolution, as discussed in the text, is shown as the red line.

forming S (^{3}P), where its associated fine-structure is much better resolved than in Fig. 2 (as expected). The low eBE portion of the broad spectrum from Fig. 2 now also shows some more defined structure. The prominent peaks from approximately 2.4 to 2.6 eV are spaced by about 30 meV (or 240 cm^{-1}). There are also some photoelectron signals under the S^- peaks and perhaps to lower the eBE. It is difficult to locate a clear structure to lower the binding energy than the set of peaks between 2.4 and 2.6 eV. Interestingly, there is a pattern to these sets of peaks. Specifically, starting with the peak at approximately 2.38 eV, the observed peaks alternate between a single narrow (close to resolution limited) peak, and what appears to be a closely spaced trio of peaks. The narrow peaks are separated by 60 meV, which corresponds to approximately 480 cm^{-1}.

The SNO^- photoelectron spectrum simulation is overlaid on the experimental spectrum in Fig. 3, where the convolution has been adjusted for the improved experimental resolution. There is surprisingly good agreement with the experimental spectrum, given the large degree of geometry change between the anion and neutral and the resulting spectral congestion. For example, the peaks from 2.38 eV to 2.6 eV in the simulation match the alternating pattern seen in the experiment. As expected, based on the large SNO angle change, these peaks all involve the SNO bending vibration. The narrow peaks in the simulation, which match the narrow (close to resolution limited) peaks in the experimental spectrum, arise from transitions of the ground vibrational state of the anion to combination bands of the SNO bend with the SN stretch in the radical neutral. Specifically, the peak at 2.38 eV is the transition to $1\nu_2 + 2\nu_3$, the peak at 2.45 eV is the transition to $1\nu_2 + 3\nu_3$, and the peak at 2.51 eV is the transition to $1\nu_2 + 4\nu_3$. Recall that these peaks in the experimental spectrum are spaced by 60 meV or 480 cm^{-1}. This is in good agreement with the calculated harmonic frequency (510 cm^{-1}), corresponding the bending vibration.

The pattern of a trio of peaks in the experimental spectrum is also seen in the simulated spectrum, although the simulated spectrum shows a doublet rather than a trio of peaks. In the simulation, these sets of peaks are made up of transitions from the ground vibrational state of the anion to increasing excitation in the SNO bend in the neutral (the peak to lower eBE), along with combination bands of the neutral SNO bend plus two quanta of the SN stretch (the peak to higher eBE). For example, the largest FCFs in the simulation for the doublet near 2.415 eV are $4\nu_3$ and $2\nu_2 + 1\nu_3$. The next duo of peaks in this sequence (near 2.475 eV) increases the number of quanta in the neutral bending excitation by one (so $5\nu_3$ and $2\nu_2 + 2\nu_3$).

While there is fairly good agreement between the experiment and theory, there is clearly more spectral congestion in the experiment, or perhaps even a broad underlying envelope, which is not captured in the simulation. This can especially be seen at higher binding energy in Fig. 2, where the S^- (^{2}P) photodetachment to form S (^{1}D) has more peaks around it than expected, along with a vertical offset in its amplitude. This is also true at the low eBE portion of the spectrum, seen in both Figs. 2 and 3, where there appears to be the photoelectron signal above the baseline extending to lower eBE than the

peaks assigned to the S^- (^2P) photodetachment to form S (^3P). With a broad, congested spectrum such as what is observed, the EA peak could be significantly lower in intensity than the peak intensity of the overall spectrum.[39] From the convolved simulation, the peak corresponding to the EA(SNO) is approximately 8000 times smaller than the peak of the photoelectron spectrum near 2.7 eV. In addition, the detachment from S^- might be obscuring the EA of SNO, just as it is certainly obscuring the low eBE portion of the spectrum. Using a lower photon energy was attempted (532 nm, 2.33 eV). However, the photodetachment signal was very small and significantly obscured by the large detachment signal from S^-, and so it was unable to be determined if there was a structure present. Even though a peak could not be assigned to the EA, an approximation can be made for the EA(SNO) based on the agreement between the simulation and the experiment. The simulation was originally shifted by +50 meV to match the peak intensity of the experimental spectrum near 2.7 eV (VDE), giving a calculated EA(SNO) = 2.16 eV. The low energy portion of the spectrum should be a better indicator of the agreement between the experiment and simulation since it will be less affected by the harmonic approximation employed in the calculation of the FCFs. As seen in Fig. 3, this EA(SNO) = 2.16 matches the higher resolution experimental spectrum quite well, particularly where there is a noticeable resolved structure.

The peaks assigned to the photodetachment from S^- in the SNO^- photoelectron spectrum are another aspect which complicates the analysis. It is highly unlikely that m/z = 62 is simply S^- in a weakly bound complex with NO, since this would likely cause a shift of the S^- photoelectron spectrum to a higher binding energy, which is not observed. In order to see the S^- photodetachment at m/z = 62, this signal likely arises from a multiphoton process: SNO^- absorbs a photon, causing excitation to an electronic excited state, which then dissociates forming S^- + NO. The S^- then absorbs a second photon, causing electron detachment. This means that there is a competition between the electronic absorption (and subsequent dissociation) and photodetachment from SNO^-. This phenomenon is also seen in other anions, such as O_3^-.[40] According to the calculations performed here (EOMCCSD/aug-cc-pVQZ) and previously,[19] SNO^- has several low-lying electronic states which could be the cause of this.

While it is highly unlikely that NOS^- was formed and stabilized in our ion source, the experimental photoelectron spectrum has too much spectral congestion to completely negate this possibility. The photodetachment from NOS^- would also give rise to a very broad, congested spectrum (shown in the supplementary material). The calculated EA(NOS) is 2.183 eV, which is very similar to the calculated EA(SNO). In addition, there are several low-lying excited electronic states in NOS^- which could generate the S^- photodetachment signal observed via a multiphoton process. Since there are no peaks able to be definitively assigned to either isomer, it is difficult to assign the observed spectrum to only SNO^- or NOS^-, and perhaps some of the observed congestion and breadth of the spectrum are due to the presence of both isomers. However, the overall good agreement between experiment and theory for SNO^- despite the significant spectral congestion, along with the slightly endothermic reaction for forming NOS^- in our ion source, indicates that SNO^- should be the dominant isomer present.

IV. DISCUSSION

A. Thermochemistry of HNSO

The NSO^- anion was successfully produced in our ion source. The reaction of NH_2^- with SO_2 does indeed produce NSO^-, as predicted by Bierbaum *et al.*,[31] with no evidence for other isomers in the reported spectrum. With the measurement of the EA(NSO) in this work and the $\Delta_{acid}H^o_{298\,K}$ from Bierbaum *et al.*,[31] a thermodynamic cycle can be used to obtain D_0(HNSO)

$$D_0\,(\mathrm{HNSO}) = \Delta_{acid}H^o_{0\,K}\,(\mathrm{HNSO}) + \mathrm{EA}\,(\mathrm{NSO}) - \mathrm{IE}\,(\mathrm{H})\,.$$

Here, D_0(HNSO) refers to the H–NSO dissociation, $\Delta_{acid}H^o_{0\,K}$(HNSO) is the 0 K gas phase acidity, the EA(NSO) is from this work, and IE(H) = 13.598 44 eV. The $\Delta_{acid}H^o_{298\,K}$(HNSO) = 344(5) kcal/mol[31] is converted to $\Delta_{acid}H^o_{0\,K}$(HNSO) from calculated heat capacities (B3LYP/aug-cc-pVQZ) using the relation

$$\Delta_{acid}H^o_{0\,K}\,(\mathrm{HNSO}) = \Delta_{acid}H^o_{298\,K}\,(\mathrm{HNSO}) - \int_0^{298}\left[C_p(\mathrm{NSO}^-) + C_p\,(\mathrm{H}^+) - C_p\,(\mathrm{HNSO})\right]dT.$$

This small thermal correction results in $\Delta_{acid}H^o_{0\,K}$ = 343(5) kcal/mol. Combining this value with the thermochemical cycle gives D_0(HNSO) = 102(5) kcal/mol or 4.4(2) eV.

B. Further analysis of the NSO^- photoelectron spectrum

The only previous measurements of the NSO vibrational frequencies were done in matrix isolation studies. The current gas phase measurements obtained from the NSO^- photoelectron spectrum are free from any matrix perturbations and include the measurement of the bending vibration which was previously not able to be observed. The current study also unambiguously assigns the three vibrational frequencies, clearing up any questions raised in the analysis of the previous matrix studies. A summary of the experimental results is in Table III.

The earliest studies by Tchir and Spratley attributed a vibrational band at 1190 cm^{-1} to NSO, arising from the VUV photolysis of HNSO in an Ar matrix. Through series of arguments, they rationalized this would be labeled as the SO stretch. This is very close to the gas phase measurement of 1202(6) for the asymmetric stretch measured here. Based on the displacement vectors from the calculations reported here (see the supplementary material), this could also be referred to as the SO stretch, agreeing with the earliest assignment of this vibrational frequency. The most recent matrix isolation studies by Wu *et al.* used both neon and argon matrices, generating NSO from the decomposition of sulfinyl azide. Using a neon matrix, their measurement of ν_1 = 1199.3 cm^{-1} is very close to our gas-phase measurement of 1202(6) cm^{-1}. They also observed ν_2 = 995.4 cm^{-1}, close to our measurement of 1010(10) cm^{-1}. However, they misidentified these

TABLE III. Summary of experimental results from the NSO^- photoelectron spectrum.

	NSO^- (cm^{-1})	NSO (cm^{-1})
ν_1	1280(30)	1202(6)
$2\nu_1$	...	2394(6)
ν_2	990(20)	1010(10)
ν_3	480(10)	300(7)
$2\nu_3$	910(20)	593(7)
$\nu_1 + \nu_3$	...	1508(8)
$\nu_1 + 2\nu_3$	...	1822(7)

EA(NSO) = 3.113(1) eV
$\Delta_{acid}H^o_{0\,K}$(HNSO) = 343(5) kcal/mol
D_0(HNSO) = 102(5) kcal/mol

two modes as the symmetric and asymmetric stretching vibrations, respectively (however, they were correctly labeled for the anion in their cited Ref. 24). The ν_1 vibration is the asymmetric stretching vibration, while ν_2 is the symmetric stretch. Our assignment is consistent with what is expected based on physical arguments for the photoelectron spectrum of NSO^-, as well as the calculations reported here. Of course, as mentioned previously, labelling ν_1 and ν_2 the asymmetric and symmetric stretches is just an approximation, albeit a very good approximation for a molecule like NSO. From the calculations here (B3LYP/aug-cc-pVQZ), the displacement vectors indicate that ν_1 (calc. 1199 cm^{-1}) could be referred to as the SO stretch and ν_2 (calc. 1017 cm^{-1}) as the SN stretch. Again, these displacement vectors are shown in the supplementary material.

While there is overall excellent agreement between the experimental results and the theoretical calculations performed here (and the subsequent photoelectron spectrum simulation), it is informative to comment on some of the small differences. This comparison or any suggested changes to the simulation do not change the results presented here for NSO^- or NSO, which are found directly from the experimental data. Instead, the purpose of this discussion is to suggest ways the theoretical treatment of NSO^-/NSO could be improved. One disagreement between the experiment and the photoelectron simulation is the intensity of the peaks corresponding to transitions involving the bending vibration (such as peak a). The calculated FCFs are less intense than the experimental results. This indicates that there should be a larger change in the NSO angle between the anion and neutral molecules than what is calculated. At the current level of theory (B3LYP/aug-cc-pVQZ), there is a 0.4° change between the anion and neutral. A least-squares fitting procedure within the PESCAL program can be used to derive the extent of the bond angle change between the anion and neutral based on fitting the simulation to the experimental photoelectron spectrum.[35] The calculated FCFs are related to the change in the normal mode geometry displacements between the anion and neutral molecules. The displacement is optimized in a least-squares fitting procedure so that the associated FCFs match the experimental peak intensities. From this procedure, the derived change in the bond angle is approximately +1.6°. Since a radical neutral is nontrivial for quantum chemical calculations, it is more likely that the neutral bond angle is the source of the discrepancy between the theory and experiment. With the anion angle held at the calculated 123.2°, the neutral angle is 124.8°. There is also more Franck-Condon activity in the asymmetric stretching vibrations in the simulation compared to the experiment (peaks e and i). This means that the change in either (or both) the NS or SO bond lengths between the anion and neutral is overestimated in the calculation compared to the experiment. Unfortunately, interpreting the outcome from using a similar PESCAL simulation fitting procedure is nontrivial because the asymmetric stretch is sensitive to the relative change along two internal coordinates (NS and SO bond lengths). A small part of this disagreement, particularly for peak i, is mitigated by using a higher photon energy (as seen in the supplementary material).

Another disagreement is the simulated population in excited anion vibrational levels. Clearly, there are several peaks lower in eBE than the EA that are in the experimental spectrum but are not captured in the simulation. The simulation was held to a Boltzmann population distribution at 200 K. In order for the intensities of the overtone transitions from the excited anion ν_1 and ν_2 to match the experiment (peaks d′ and e′), without changing the FCFs, a Boltzmann temperature would have to be close to 450 K, significantly higher than what is expected. Keep in mind that NSO^- is likely formed in our ion source from the reaction of NH_2^- with SO_2, a reaction that is exothermic by ≤46 kcal/mol (≤2 eV).[31] A simple Boltzmann vibrational population distribution is likely not appropriate for this ion source, given that this source relies on a supersonic jet expansion for both the reaction and subsequent collisional stabilization and cooling.

The NSO^- photoelectron spectrum can be compared to that of NCO^-.[41] For NCO^-, a similar bonding motif is expected, where the partial positive charge is on the central atom and partial negative charges are on the terminal N and O atoms. The difference between the anion and neutral geometries is also very similar, where the NC bond lengthens and the CO bond contracts on removal of an electron. However, both NCO and NCO^- are linear, so there are no analogous bending mode excitations. Despite the bond angle difference, the photoelectron spectra of NSO^- and NCO^- appear to be very similar, albeit with a different electron affinity, where the EA(NCO) = 3.609(5) eV. Another point of comparison is between NSO^- and NOO^-, the peroxy form of NO_2^-. The peroxy form of NO_2^- was suggested to exist in the photodetachment studies by Adams *et al.*,[42] Richards *et al.*,[43] and then by Herbst *et al.*[44] Since NSO^- is valence isoelectronic with the NOO^- anion, it might be expected to have similar bonding character or structure given the similarities between oxygen and sulfur. However, the difference in electronegativity between oxygen and sulfur as the central atom is likely enough to stabilize NSO^- and the corresponding radical neutral, forming a covalently bound triatomic. This is in contrast to the suggested dissociation of NOO^- to form NO + O plus a free electron, along with the proposed NOO^- structure being more similar to an $NO\ldots O^-$ electrostatic interaction than to a covalent bond.[44]

V. CONCLUSION

The photoelectron spectra of NSO^- and SNO^- were measured. Isomer-specific ion generation was achieved by the rational ion synthesis capability in our dual pulsed valve plasma entrainment source. All of the fundamental vibrational frequencies of NSO and NSO^- were measured, along with EA(NSO) = 3.113(1) eV. Several overtone vibrational frequencies were also measured for NSO. The NSO vibrational frequencies were unambiguously assigned to the mode descriptions. In addition, the vibrational mode assignments make physical sense based on what is expected in the NSO^- photoelectron spectrum. The H–NSO bond dissociation energy was also derived as $D_0(HNSO) = 102(5)$ kcal/mol using a thermochemical cycle and the previously measured $\Delta_{acid}H^{o}_{298\ K}$ (HNSO). There are stark differences between the NSO^- and SNO^- photoelectron spectra, namely, in the level of spectral congestion. While the NSO^- photoelectron spectrum was relatively sparse, indicative of little change between the anion and neutral equilibrium geometries, the SNO^- spectrum was so congested that little spectroscopic information could be gained from it. In addition, a multiphoton process, where SNO^- photodissociates to form S^- + NO followed by the S^- photodetachment, further complicated the analysis of the SNO^- photoelectron spectrum. While it is unlikely that NOS^- was formed and stabilized in our ion source, it cannot be completely negated and might contribute to the observed spectrum. However, there was relatively good agreement between the experimental and theoretical results, and combined with energetic arguments, it was most likely that SNO^- was responsible for the observed photoelectron spectrum. An approximate EA(SNO) was found to be 2.16 eV, and the bending vibrational frequency of SNO (ν_3) was estimated to be 480 cm^{-1}. Additional higher level calculations would be useful to further analyze the SNO^- photoelectron spectrum, particularly to model the congested photoelectron spectrum to gain a more accurate EA(SNO) and to better understand the presence of the multiphoton photoelectron signal.

SUPPLEMENTARY MATERIAL

See supplementary material for an additional photoelectron spectrum of NSO^- using a higher photon energy, descriptions and displacement vectors for the NSO and NSO^- vibrational modes, and a simulated photoelectron spectrum of NOS^-.

ACKNOWLEDGMENTS

The authors gratefully acknowledge support from NSF Grant No. PHY1125844 for significant contributions to this project.

[1]T. Chivers, *A Guide to Chalcogen-Nitrogen Chemistry* (World Scientific Publishing Co., New Jersey, 2005).
[2]M. M. Cortese-Krott, A. R. Butler, J. D. Woollins, and M. Feelisch, Dalton Trans. **45**, 5908 (2016).
[3]M. M. Cortese-Krott, B. O. Fernandez, M. Kelm, A. R. Butler, and M. Feelisch, Nitric Oxide **46**, 14 (2015).
[4]M. M. Cortese-Krott, B. O. Fernandez, J. L. T. Santos, E. Mergia, M. Grman, P. Nagy, M. Kelm, A. Butler, and M. Feelisch, Redox Biol. **2**, 234 (2014).
[5]M. M. Cortese-Krott, G. G. C. Kuhnle, A. Dyson, B. O. Fernandez, M. Grman, J. F. DuMond, M. P. Barrow, G. McLeod, H. Nakagawa, K. Ondrias, P. Nagy, S. B. King, J. E. Saavedra, L. K. Keefer, M. Singer, M. Kelm, A. R. Butler, and M. Feelisch, Proc. Natl. Acad. Sci. U. S. A. **112**, E4651 (2015).
[6]R. Wedmann, A. Zahl, T. E. Shubina, M. Durr, F. W. Heinemann, B. E. C. Bugenhagen, P. Burger, I. Ivanovic-Burmazovic, and M. R. Filipovic, Inorg. Chem. **54**, 9367 (2015).
[7]R. M. Romano and C. O. Della Vedova, J. Mol. Struct. **522**, 1 (2000).
[8]L. Puskar, E. G. Robertson, and D. McNaughton, J. Mol. Spectrosc. **240**, 244 (2006).
[9]M. Hochlaf, R. Linguerri, and J. S. Francisco, J. Chem. Phys. **139**, 234304 (2013).
[10]M. Mendez, J. S. Francisco, and D. A. Dixon, Chem. Eur. J. **20**, 10231 (2014).
[11]R. Labbow, D. Michalik, F. Reiss, A. Schulz, and A. Villinger, Angew. Chem., Int. Ed. **55**, 7680 (2016).
[12]L. V. Ivanova, B. J. Anton, and Q. K. Timerghazin, Phys. Chem. Chem. Phys. **16**, 8476 (2014).
[13]P. O. Tchir and R. D. Spratley, Can. J. Chem. **53**, 2318 (1975).
[14]P. O. Tchir and R. D. Spratley, Can. J. Chem. **53**, 2331 (1975).
[15]Z. Wu, D. Q. Li, H. M. Li, B. F. Zhu, H. L. Sun, J. S. Francisco, and X. Q. Zeng, Angew. Chem., Int. Ed. **55**, 1507 (2016).
[16]L. Andrews, P. Hassanzadeh, G. D. Brabson, A. Citra, and M. Neurock, J. Phys. Chem. **100**, 8273 (1996).
[17]M. Bahou and Y. P. Lee, J. Chem. Phys. **115**, 10694 (2001).
[18]M. Hawkins and A. J. Downs, J. Phys. Chem. **88**, 3042 (1984).
[19]T. Trabelsi, O. Yazidi, J. S. Francisco, R. Linguerri, and M. Hochlaf, J. Chem. Phys. **143**, 164301 (2015).
[20]O. Yazidi, A. Ben Houria, J. S. Francisco, and M. Hochlaf, J. Chem. Phys. **138**, 104318 (2013).
[21]D. S. Bohle, C. H. Hung, and B. D. Smith, Can. J. Chem. **83**, 2021 (2005).
[22]T. Chivers, A. B. F. Dasilva, O. Treu, and M. Trsic, J. Mol. Struct. **162**, 351 (1987).
[23]C. Ehrhardt and R. Ahlrichs, Chem. Phys. **108**, 417 (1986).
[24]R. C. Fortenberry and J. S. Francisco, J. Chem. Phys. **143**, 184301 (2015).
[25]L. Sheps, E. M. Miller, and W. C. Lineberger, J. Chem. Phys. **131**, 064304 (2009).
[26]Y.-J. Lu, J. H. Lehman, and W. C. Lineberger, J. Chem. Phys. **142**, 044201 (2015).
[27]A. Eppink and D. H. Parker, Rev. Sci. Instrum. **68**, 3477 (1997).
[28]V. Dribinski, A. Ossadtchi, V. A. Mandelshtam, and H. Reisler, Rev. Sci. Instrum. **73**, 2634 (2002).
[29]C. Blondel, W. Chaibi, C. Delsart, C. Drag, F. Goldfarb, and S. Kroger, Eur. Phys. J. D **33**, 335 (2005).
[30]H. Hotop and W. C. Lineberger, J. Phys. Chem. Ref. Data **14**, 731 (1985).
[31]V. M. Bierbaum, J. J. Grabowski, and C. H. Depuy, J. Phys. Chem. **88**, 1389 (1984).
[32]J. M. Van Doren, A. A. Viggiano, R. A. Morris, A. E. S. Miller, T. M. Miller, J. F. Paulson, C. A. Deakyne, H. H. Michels, and J. A. Montgomery, J. Chem. Phys. **98**, 7940 (1993).
[33]M. J. Frisch, G. W. Trucks, H. B. Schlegel, G. E. Scuseria, M. A. Robb, J. R. Cheeseman, G. Scalmani, V. Barone, B. Mennucci, G. A. Petersson, H. Nakatsuji, M. Caricato, X. Li, H. P. Hratchian, A. F. Izmaylov, J. Bloino, G. Zheng, J. L. Sonnenberg, M. Hada, M. Ehara, K. Toyota, R. Fukuda, J. Hasegawa, M. Ishida, T. Nakajima, Y. Honda, O. Kitao, H. Nakai, T. Vreven, J. A. Montgomery, Jr., J. E. Peralta, F. Ogliaro, M. J. Bearpark, J. Heyd, E. N. Brothers, K. N. Kudin, V. N. Staroverov, R. Kobayashi, J. Normand, K. Raghavachari, A. P. Rendell, J. C. Burant, S. S. Iyengar, J. Tomasi, M. Cossi, N. Rega, N. J. Millam, M. Klene, J. E. Knox, J. B. Cross, V. Bakken, C. Adamo, J. Jaramillo, R. Gomperts, R. E. Stratmann, O. Yazyev, A. J. Austin, R. Cammi, C. Pomelli, J. W. Ochterski, R. L. Martin, K. Morokuma, V. G. Zakrzewski, G. A. Voth, P. Salvador, J. J. Dannenberg, S. Dapprich, A. D. Daniels, Ö. Farkas, J. B. Foresman, J. V. Ortiz, J. Cioslowski, and D. J. Fox, GAUSSIAN 09, Revision B.01, Gaussian, Inc., Wallingford, CT, USA, 2009.
[34]K. M. Ervin, T. M. Ramond, G. E. Davico, R. L. Schwartz, S. M. Casey, and W. C. Lineberger, J. Phys. Chem. A **105**, 10822 (2001).
[35]K. M. Ervin, J. Ho, and W. C. Lineberger, J. Phys. Chem. **92**, 5405 (1988).
[36]P. C. Engelking, J. Phys. Chem. **90**, 4544 (1986).
[37]C. M. Western, PGOPHER, a program for simulating rotational, vibrational and electronic spectra, University of Bristol, http://pgopher.chm.bris.ac.uk.
[38]A. Sanov, Annu. Rev. Phys. Chem. **65**, 341 (2014).

[39]S. W. Wren, K. M. Vogelhuber, K. M. Ervin, and W. C. Lineberger, Phys. Chem. Chem. Phys. **11**, 4745 (2009).
[40]S. E. Novick, P. C. Engelking, P. L. Jones, J. H. Futrell, and W. C. Lineberger, J. Chem. Phys. **70**, 2652 (1979).
[41]S. E. Bradforth, E. H. Kim, D. W. Arnold, and D. M. Neumark, J. Chem. Phys. **98**, 800 (1993).
[42]N. G. Adams, D. K. Bohme, D. B. Dunkin, F. C. Fehsenfeld, and E. E. Ferguson, J. Chem. Phys. **52**, 3133 (1970).
[43]J. H. Richards, L. M. Stephens, and J. I. Brauman, Chem. Phys. Lett. **25**, 318 (1974).
[44]E. Herbst, T. A. Patterson, and W. C. Lineberger, J. Chem. Phys. **61**, 1300 (1974).